Ground- and excited-rovibrational-state properties of weakly bound helium-silver triatomic molecules

Hiroya Suno ●*

Research Center for Computing and Multimedia Studies, Hosei University, 3-7-2 Kajino-cho, Koganei-shi, Tokyo 184-8584, Japan

Ground and excited-rovibrational states of weakly bound triatomic molecules containing two helium and one silver atoms are investigated. We consider three systems, ^{4}He - ^{4}He -Ag, ^{3}He - ^{4}He -Ag, and ^{3}He - ^{3}He -Ag. The three-atom Schrödinger equation is solved in hyperspherical coordinates using the potential-energy surface represented as the addition of He-He and He-Ag pair interaction potentials. We compute the energy levels and analyze the structural properties by considering averaged pair distances and bond angles, one-dimensional pair and angle distribution functions, and two-dimensional pair-pair and angle-angle distribution functions. All the He-He-Ag bound states are found to possess similar characteristics, displaying obtuse isosceles (^{4}He$_2$Ag and ^{3}He$_2$Ag) or scalene (^{3}He ^{4}HeAg) triangle configurations where the He-Ag distances are nearly fixed and the Ag bond angle is variable.

I. INTRODUCTION

Triatomic systems containing helium have attracted much interest in the past decades due to the possibility of observing unique quantum properties like the Efimov effect [1–4]. One of the best candidates for this phenomenon is the ^{4}He trimer, ^{4}He$_3$, whose excited state is of Efimov character [5,6]. The first successful experiments on the ^{4}He trimer excited state were reported in Ref. [7]. The ^{4}He trimer and its isotopes have therefore been the subject of most extensive theoretical study, see the pioneering paper in Ref. [8] and the subsequent papers in Refs. [5,8–11]. The ^{4}He trimer is found to support two weakly bound states while its isotope, ^{3}He ^{4}He$_2$, is shown to support only one loosely bound state [9]. In addition to the helium trimers studied so far, there exist other interesting examples of weakly bound triatomic molecules. The He$_2$Li systems, as well as other He-He-alkali-metal systems, are also known to support weakly bound states, and were studied by several authors [12–22]. The He$_2$Ca systems were investigated by Gou and Li [23] and López-Durán *et al.* [24,25]. The ground and excited-rovibrational states of such weakly bound molecules are found to extend far into the classically forbidden regions, allowing for testing "universality" predicted for these "quantum halo states" [18].

Triatomic molecules formed with two He atoms and an impurity can also be interpreted as extreme limiting cases of large helium droplets [26–29]. The shifts of the electronic transition lines with respect to the isolated atom determine the location of the impurity attached to a droplet. The issue of establishing solvation instead of surface location for an impurity atom in a helium droplet is, therefore, of great importance to further understand the behavior of the spectroscopic observations as a function of the droplet's size. While

most atomic and molecular impurities are found to reside in the interior [30], it is well established that, according to the model of Ref. [31], alkali-metal atoms preferentially reside in a "dimple" at the surface of the droplets for both helium isotopes [28,32]. It was also established that Ca atoms reside on the surface of superfluid boson helium nanodroplets [33], in agreement with density functional theory [34]. On the other hand, silver atoms are shown to be attracted to the helium enough to locate inside the boson helium droplets [35], although they move to the surface and desorb [36–38] after photoexcitation Ag($5p$ ^2P_J) ← Ag($5s$ $^2S_{1/2}$). Therefore, a knowledge of the precise preferred location of the impurity with respect to the surrounding pair of He atoms in the triatomic system is expected to provide some insights into the intrinsic nature of their interaction with the rare gas. Lastly, such triatomic systems are also relevant to buffer-gas experiments performed on cold molecules by Brahms *et al.* [39], in which the AgHe molecular species was observed to form via three-body recombination Ag + He + He → AgHe + He.

This work is along the lines of previous investigations which dealt with weakly bound triatomic helium-helium-impurity systems. We study in detail the ground and excited-rovibrational states of helium-helium-silver molecules. Three systems, ^{4}He - ^{4}He -Ag, ^{3}He - ^{4}He -Ag, and ^{3}He - ^{3}He -Ag, are considered with different total angular momenta J and parities Π. For ^{3}He - ^{3}He -Ag, the spatial wave function is assumed to be symmetric under the exchange of the two ^{3}He atoms, corresponding with their singlet nuclear spin state $I_{3\mathrm{He}3\mathrm{He}} = 0$. The three-atom Schrödinger equation in hyperspherical coordinates is solved by using an expansion of the wave function on the adiabatic channel functions at fixed finite-element-method-discrete-variable-representation (FEM-DVR) grid points [40] together with the potential-energy surface represented as the addition of He-He and He-Ag pair interaction potentials. We calculate the energy levels and analyze the structural properties by considering

---

*hiroya.suno.73@hosei.ac.jp

averaged pair distances and bond angles, one-dimensional (1D) pair and angle distribution functions, and two-dimensional (2D) pair-pair and angle-angle distribution functions.

The organization of this paper is as follows. Section II presents the theoretical approach. In Sec III, we discuss the results and analyses of the systems under study. We finally conclude and summarize in Sec IV.

II. METHOD

The Schrödinger equation is solved for three interacting atoms in hyperspherical coordinates [41] using the slow variable discretization (SVD) approach [42–44]. After separation of the center-of-mass motion, the three-body problem can be described using a modified version of Whitten-Smith's democratic hyperspherical coordinates $(R, \Omega) \equiv (R, \theta, \varphi, \alpha, \beta, \gamma)$ [45,46]. The Euler angles (α, β, γ) describe the orientation of the body-fixed frame in space. The hyperradius R characterizes the global size of the triatomic system, while the two hyperangles (θ, φ) specify the shape of the molecular triangle. The hyperangle θ is defined in the range $[0, \pi/2]$, with $\theta = 0$ and $\pi/2$ corresponding, respectively, with equilateral and collinear triangles. The hyperangle φ is restricted to the range $[0, 2\pi]$, after we required the wave function to be single-valued. The hyperangle φ can be further restricted to the range $[0, \pi]$ in the case of two identical atoms contained in the system.

Using a rescaled wave function $\psi = R^{5/2}\Psi$, with Ψ being the usual solution, the Schrödinger equation for the three atoms interacting through the potential-energy surface $V(R, \theta, \varphi)$ is given by

$$\left[-\frac{\hbar^2}{2\mu} \frac{\partial^2}{\partial R^2} + \frac{\hat{\Lambda}^2}{2\mu R^2} + \frac{15\hbar^2}{8\mu R^2} + V(R, \theta, \varphi) \right] \psi(R, \Omega)$$
$$= E\psi(R, \Omega), \tag{1}$$

where

$$\hat{\Lambda}^2 = -\frac{4\hbar^2}{\sin 2\theta} \frac{\partial}{\partial \theta} \sin 2\theta \frac{\partial}{\partial \theta} + \frac{4}{\sin^2 \theta} \left(i\hbar \frac{\partial}{\partial \varphi} - \cos\theta \frac{J_z}{2} \right)^2$$
$$+ \frac{2J_x^2}{1 - \sin\theta} + \frac{2J_y^2}{1 + \sin\theta} + J_z^2 \tag{2}$$

is the squared grand angular momentum operator, (J_x, J_y, J_z) the body-fixed frame (x, y, z) components of the total angular momentum $\mathbf{J}$, and

$$\mu = \sqrt{\frac{m_1 m_2 m_3}{m_1 + m_2 + m_3}} \tag{3}$$

the three-body reduced mass with m_i being the atoms' respective masses.

In solving the Schrödinger Eq. (1), we expand the wave function ψ on a product basis [42]

$$\psi(R, \Omega) = \sum_{\nu, l} c_{\nu l} \chi_l(R) \Phi_\nu(R_l; \Omega), \tag{4}$$

where Φ_ν are the channel functions labeled ν ($\nu = 1, 2, \dots,$), which will be defined below. The $c_{\nu l}$ are the expansion coefficients, and $\chi_l(R)$ represent the FEM-DVR basis functions

[40], which are obtained from sets of Lobatto shape functions on a grid of hyperradial points R_l in the range $[R_{\min}, R_{\max}]$. The grid points and the associated weights (R_l, ω_l) are generated by dividing the range with a set of N grid points and by dividing each interval again with shifting and scaling of the $\mathcal{M}$th-order Gauss-Lobatto quadrature [47]. The total number of hyperradial grid points amounts to $L = (\mathcal{M} - 1)(N - 1) + 1$ with any two repeated points being merged into one single point.

The channel functions Φ_ν ($\nu = 1, \dots, \nu_{\max}$) in Eq. (4) are solutions of the adiabatic Schrödinger equation

$$\left[\frac{\Lambda^2}{2\mu R^2} + \frac{15\hbar^2}{8\mu R^2} + V(R, \theta, \varphi) \right] \Phi_\nu(R; \Omega) = U_\nu(R)\Phi_\nu(R; \Omega), \tag{5}$$

and are needed only at the hyperradial grid points $R = R_l$. The adiabatic hyperspherical potential curves $U_\nu(R)$ contain useful information to gain insight into the energetic structure of the three-body system. Equation (5) is solved by expanding the channel function on the normalized Wigner functions $\tilde{D}_{KM}^J(\alpha, \beta, \gamma) = [(2J + 1)/8\pi]^{1/2} D_{KM}^J(\alpha, \beta, \gamma)$:

$$\Phi_\nu^{JM\Pi}(R; \Omega) = \sum_K \phi_{K\nu}^{J\Pi}(R; \theta, \varphi) \tilde{D}_{KM}^J(\alpha, \beta, \gamma), \tag{6}$$

where K, denoting the projection of $\mathbf{J}$ on a body-fixed axis, takes on the integer values that satisfy $-J \leqslant K \leqslant K$ and $\Pi = (-1)^K$. For a system comprising three nonidentical atoms, the solution of the adiabatic Eq. (5) must satisfy the boundary conditions

$$(-1)^K \phi_{K\nu}(R; \theta, 0) = \phi_{K\nu}(R; \theta, 2\pi), \tag{7}$$

$$(-1)^K \left. \frac{\partial \phi_{K\nu}}{\partial \varphi} \right|_{\varphi=0} = \left. \frac{\partial \phi_{K\nu}}{\partial \varphi} \right|_{\varphi=2\pi}. \tag{8}$$

On the other hand, for a system containing two identical atoms for which the wave function is symmetric under exchange, the permutation symmetry can be taken into account via the boundary conditions

$$(-1)^{J+K} \phi_{-K\nu}(R; \theta, 0) = \phi_{K\nu}(R; \theta, 0), \tag{9}$$

$$(-1)^{J+K+1} \left. \frac{\partial \phi_{-K\nu}}{\partial \varphi} \right|_{\varphi=0} = \left. \frac{\partial \phi_{K\nu}}{\partial \varphi} \right|_{\varphi=0}, \tag{10}$$

$$(-1)^J \phi_{-K\nu}(R; \theta, \pi) = \phi_{K\nu}(R; \theta, \pi), \tag{11}$$

$$(-1)^{J+1} \left. \frac{\partial \phi_{-K\nu}}{\partial \varphi} \right|_{\varphi=\pi} = \left. \frac{\partial \phi_{K\nu}}{\partial \varphi} \right|_{\varphi=\pi}, \tag{12}$$

and the hyperangle φ is now restricted to the range $[0, \pi]$. The $\phi_{K\nu}(R; \theta, \varphi)$ in Eq. (6) is expanded on a direct product of fifth-order basis splines [48] in θ and φ generated from N_θ and N_φ mesh points, respectively.

Inserting ψ of Eq. (4) into the Schrödinger Eq. (1), we obtain a set of hyperradial coupled-channel equations

$$\sum_{\nu'} \sum_{l'} [\mathcal{T}_{ll'} \mathcal{O}_{\nu l, \nu' l'} + U_\nu(R_l)\delta_{\nu\nu'}\delta_{ll'}] c_{\nu' l'} = E c_{\nu l}, \tag{13}$$

where $\mathcal{O}_{\nu l, \nu' l'} = \int d\Omega \, \Phi_\nu(R_l; \Omega) \Phi_{\nu'}(R_{l'}; \Omega)$ are the overlap matrix elements between adiabatic channels defined at different hyperradial points $R = R_l$ and $R = R_{l'}$, and $\mathcal{T}_{ll'}$ are

TABLE I. Bound-state energies and s-wave scattering lengths a for the He-He and He-Ag systems.

	l	$\epsilon_{v=0,l}$ (K)	$\epsilon_{v=0,l}$ (a.u.)	a (Å)	a (a.u.)
^{4}He ^{4}He	0	-1.310	-4.148×10^{-9}	100	189
^{3}He ^{4}He	0	–	–	-17.6	-33.3
^{3}He ^{3}He	0	–	–	-7.16	-13.5
^{4}HeAg	0	-3.248	-1.028×10^{-5}	0.33	0.17
	1	-2.805	-0.883×10^{-6}	–	–
	2	-1.938	-6.136×10^{-6}	–	–
	3	-0.691	-2.188×10^{-6}	–	–
^{3}HeAg	0	-2.510	-7.948×10^{-6}	7.93	4.20
	1	-1.969	-6.234×10^{-6}	–	–
	2	-0.928	-2.938×10^{-6}	–	–

the hyperradial kinetic energy matrix elements given in Refs. [40,43]. The hyperradial Hamiltonian matrix $H_{vl,v'l'} = \mathcal{T}_{ll'}\mathcal{O}_{vl,v'l'} + U_v(R_l)\delta_{vv'}\delta_{ll'}$ possesses a symmetric banded structure due to the characteristic of the FEM-DVR basis, so that one can easily numerically solve the coupled Eqs. (13).

The potential-energy surface $V(R, \theta, \varphi)$ in Eq. (1) is represented as the addition of three pair-interaction potentials

$$V(R, \theta, \varphi) = v_{\text{HeAg}}(r_{12}) + v_{\text{HeHe}}(r_{23}) + v_{\text{HeAg}}(r_{31}), \quad (14)$$

where r_{ij} are the interatomic distances, expressed in our coordinate system as

$$r_{ij} = 2^{-1/2}d_{ij}R[1 + \sin\theta\cos(\varphi + \varphi_{ij})]^{1/2}, \quad (15)$$

with $\varphi_{12} = 2\tan^{-1}(m_2/\mu)$, $\varphi_{23} = 0$ $\varphi_{31} = -2\tan^{-1}(m_3/\mu)$, and the d_{ij} coefficients are given by

$$d_{ij} = \left[\frac{m_k(m_i + m_j)}{\mu(m_1 + m_2 + m_3)}\right]^{1/2}, \quad (16)$$

where (ijk) is a cyclic permutation of (123). For the He-He interaction, a variety of potentials are proposed in the literature, but here we adopt the most widely used LM2M2 representation developed by Aziz and Slaman [49]. This interaction potential supports one ^{4}He$_2$ zero angular momentum $l = 0$ bound state with the energy level being $\epsilon_{v=0,l=0}^{^4\text{He}^4\text{He}} = -1.310 \times 10^{-3}$K, while there exists no bound state for the isotopes ^{4}He ^{3}He and ^{3}He$_2$. For the He-Ag interaction, we adopt the analytical form proposed by Xie *et al.* in Ref. [50], obtained by fitting the best AgHe potential data of Gardner *et al.* [51]. This potential is found to support one ^{4}HeAg bound state each for $l = 0, 1, 2$, and 3, and one ^{3}HeAg bound state each for $l = 0, 1$, and 2. Table I presents the bound-state energies (in a.u. and Kelvin) as well as the relevant s-wave scattering lengths (in a.u. and Å) calculated using the R-matrix propagation method [52]. In particular, the s-wave scattering lengths of ^{3,4}He -Ag are found to be much smaller than that of ^{4}He - ^{4}He. Figure 1 shows these interaction potentials and the supported bound states' wave functions. We notice that the He-Ag wave functions are much more "compact" than the ^{4}He - ^{4}He, implying the more tightly binding nature between helium and silver.
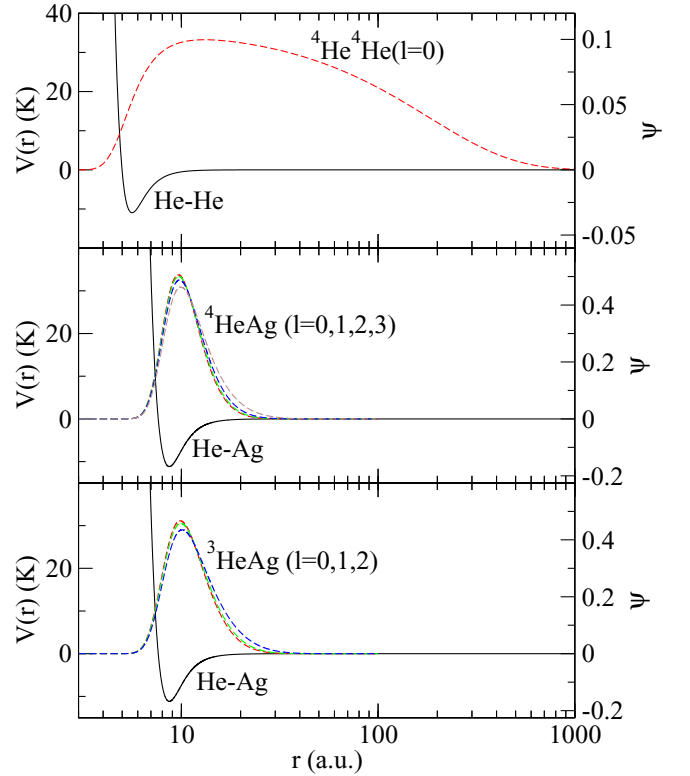

FIG. 1. He-He and He-Ag interaction potentials and the ^{4}He - ^{4}He, ^{4}He -Ag, and ^{3}He -Ag bound-state wave functions with angular momentum l supported by these potentials.

III. RESULTS

We calculated the adiabatic hyperspherical potential curves $U_v(R)$ and channel functions $\Phi_v(R; \Omega)$ for the ^{4}He$_2$Ag, ^{3}He ^{4}HeAg, and ^{3}He$_2$Ag systems with different total angular momenta J and parities Π. We show here only the $J^\Pi = 0^+$ adiabatic hyperspherical potential curves. Figures 2(a) presents the 20 lowest 0^+ adiabatic hyperspherical potential curves $U_v(R)$ ($v = 1, 2, \ldots, 20$) as functions of the hyperradius R for ^{4}He$_2$Ag. The bound-state energy levels, which will be calculated below, are indicated by horizontal lines. The lowest $v = 1$ potential curve corresponds asymptotically to one ^{4}He atom and the Ag atom bound in the zero two-body angular momentum $l = 0$ state with the other ^{4}He atom far away, approaching the ^{4}HeAg$(v = 0, l = 0) + ^4$He dissociation threshold, $\epsilon_{v=0,l=0}^{4\text{HeAg}} = -3.248$ K as $R \rightarrow \infty$. The second lowest $v = 2$ potential curve corresponds asymptotically to the $l = 1$ ^{4}HeAg bound state and the other ^{4}He atom far away, approaching ^{4}HeAg$(v = 0, l = 1) + ^4$He dissociation threshold, $\epsilon_{v=0,l=1}^{4\text{HeAg}} = -2.805$ K as $R \rightarrow \infty$. In the same way, the $v = 3$, 4, and 5 potential curves are considered to be the ^{4}HeAg$(v = 0, l = 2) + ^4$He, ^{4}HeAg$(v = 0, l = 3) + ^4$He, and ^{4}He$_2(v = 0, l = 0)$+Ag dissociation channels, respectively. The other $v \geqslant 6$ potential curves represent the three-body continuum and approach the three-body dissociation threshold $U_v(R) \rightarrow 0$ at large R. Figure 2(b) shows the 0^+ adiabatic hyperspherical potential curves as functions of the hyperradius R for ^{3}He ^{4}HeAg. The lowest $v = 1$ and second lowest $v = 2$ potential curves represent, respectively,
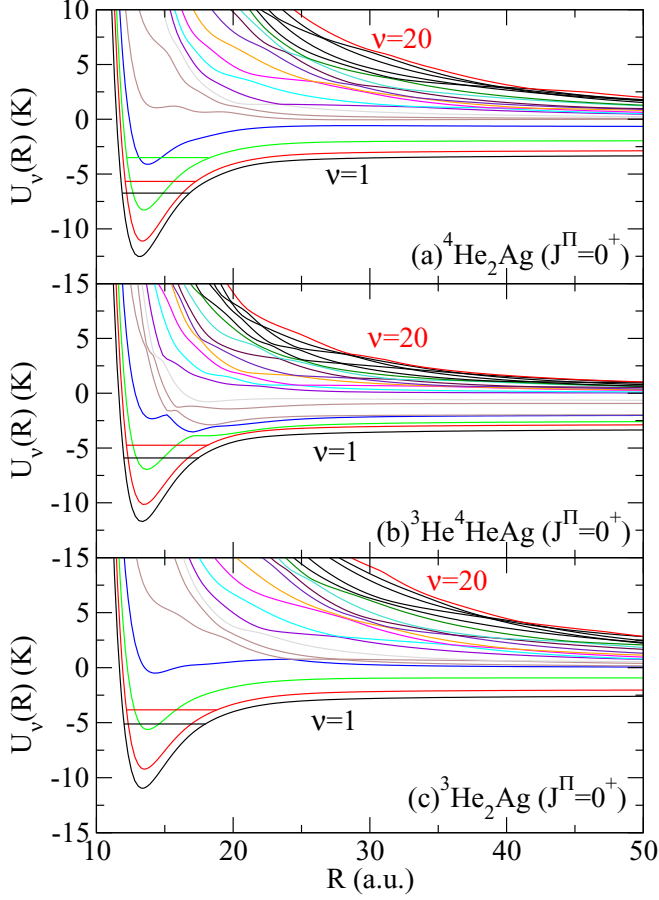
FIG. 2. The 20 lowest 0^+ adiabatic hyperspherical potential curves $U_\nu(R)$ ($\nu = 1, 2, \ldots, 20$) as functions of the hyperradius R for (a) $^4\text{He}_2\text{Ag}$, (b) $^3\text{He}^4\text{HeAg}$, and (c) $^3\text{He}_2\text{Ag}$. The horizontal lines indicate the bound-state energy levels.

the $^4\text{HeAg}(v = 0, l = 0) + \ ^3\text{He}$ and $^3\text{HeAg}(v = 0, l = 0) + \ ^4\text{He}$ dissociation channels, and the other higher potential curves can be identified in the same manner. The potential curves for $^3\text{He}_2\text{Ag}$, shown in Fig. 2(c), can be analyzed similarly. We checked the convergence of the potential curves by computing them with different numbers of hyperangular basis-splines mesh points and found that $(N_\theta, N_\varphi) = (200, 80)$ are sufficient to obtain about six digits of accuracy for several tens of the lowest potential curves.

The coupled-channel hyperradial Eqs. (13) are numerically solved with the sum over ν truncated at $\nu = \nu_{max}$ to obtain bound-state energies. In practice, at most $\nu_{max} \approx 60$ channels

and the maximum number of hyperradial FEM-DVR grid points $L \approx 250$ for $7 \lesssim R \lesssim 100$ a.u., are sufficient for four digits of accuracy for these ground and excited-rovibrational energy levels. For all the triatomic systems under study, we find bound states only for the "parity-favored" cases, i.e., $\Pi = (-1)^J$, while no bound state was seen to exist for the "parity-unfavored" cases, $\Pi = (-1)^{J+1}$. We show the $^4\text{He}_2\text{Ag}$, $^3\text{He}^4\text{HeAg}$, and $^3\text{He}_2\text{Ag}$ bound-state energy levels only for $J^\Pi = 0^+$, 1^-, and 2^+ in Table II, where the bound states are labeled by the total angular momentum J, the parity Π, and the vibrational quantum number v. We mention here that there still exist bound states with higher "parity-favored" angular momenta and parities, $J \geqslant 3$ and $\Pi = (-1)^J$, for all these triatomic isotopic species.

The averaged pair distances and bond angles are given, respectively, by

$$\langle r_{ij} \rangle = \int dR \int d\Omega \, \psi(R, \Omega)^* r_{ij} \psi(R, \Omega), \qquad (17)$$

and

$$\langle \vartheta_j \rangle = \int dR \int d\Omega \, \psi(R, \Omega)^* \cos^{-1} \frac{r_{ij}^2 + r_{jk}^2 - r_{ki}^2}{2 r_{ij} r_{jk}} \psi(R, \Omega), \tag{18}$$

where (ijk) is a cyclic permutation of (123). Table III presents these averaged values for the $J^\Pi = 0^+$, 1^-, and 2^+ bound states of $^4\text{He}_2\text{Ag}$, $^3\text{He}^4\text{HeAg}$, and $^3\text{He}_2\text{Ag}$. For all the $^4\text{He}_2\text{Ag}$ bound states, the averaged $^4\text{He}\,\text{-Ag}$ distance is found to be around 10.5 a.u., somewhat smaller than the averaged ^4He - ^4He distance, which is between about 12 to 16 a.u.. Similarly, the Ag bond angle is found to be, in general, larger than the ^4He bond angles, which can be explained from the fact that the $^4\text{He}\,\text{-Ag}$ diatomic subsystem is more tightly bound than the ^4He - ^4He subsystem; see Fig. 1. These averaged pair distances and bond angles suggest that the $^4\text{He}_2\text{Ag}$ bound states all present obtuse isosceles triangle configurations. The $^3\text{He}^4\text{HeAg}$ and $^3\text{He}_2$ bound states can be analyzed in a similar manner: the $^3\text{He}^4\text{HeAg}$ bound states show scalene triangles with $\langle r_{^4\text{HeAg}} \rangle \lesssim \langle r_{^3\text{HeAg}} \rangle < \langle r_{^3\text{He}^4\text{He}} \rangle$ or $\langle \vartheta_{^3\text{He}} \rangle \lesssim \langle \vartheta_{^4\text{He}} \rangle < \langle \vartheta_{\text{Ag}} \rangle$, while the $^3\text{He}_2\text{Ag}$ bound states present again obtuse isosceles triangles with $\langle r_{^3\text{HeAg}} \rangle < \langle r_{^3\text{He}^3\text{He}} \rangle$ or $\langle \vartheta_{^3\text{He}} \rangle < \langle \vartheta_{\text{Ag}} \rangle$.

To gain more insight into the structure of these triatomic systems, we analyze the 1D pair and angle distribution functions which can be calculated from the three-dimensional (3D)

TABLE II. Bound-state energies for the $^4\text{He}_2\text{Ag}$, $^3\text{He}^4\text{HeAg}$, and $^3\text{He}_2\text{Ag}$ complexes. The energies are given in units of Kelvin and are relative to the three-body dissociation threshold. The bound states are labeled by the total angular momentum J, the parity Π, and the vibrational quantum number v.

	$^4\text{He}_2\text{Ag}$			$^3\text{He}^4\text{HeAg}$			$^3\text{He}_2\text{Ag}$		
v	$J^\Pi = 0^+$	1^-	2^+	0^+	1^-	2^+	0^+	1^-	2^+
0	-6.739	-6.353	-5.823	-5.909	-5.329	-4.352	-5.115	-4.569	-4.014
1	-5.670	-4.612	-5.305	-4.743		-3.558	-3.834	-2.619	-3.445
2	-3.496		-4.119						

TABLE III. Average values of the pair distances (in atomic units) and the bond angles (in radians) for $^4\text{He}_2\text{Ag}$, $^3\text{He}\,^4\text{HeAg}$, and $^3\text{He}_2\text{Ag}$.

	J^Π	v	$\langle r_{4\text{HeAg}}\rangle$	$\langle r_{3\text{HeAg}}\rangle$	$\langle r_{\text{HeHe}}\rangle$	$\langle\vartheta_{\text{Ag}}\rangle$	$\langle\vartheta_{4\text{He}}\rangle$	$\langle\vartheta_{3\text{He}}\rangle$
$^4\text{He}_2\text{Ag}$	0^+	0	10.44		13.00	0.45π	0.28π	
		1	10.58		16.07	0.61π	0.19π	
		2	11.33		15.26	0.53π	0.24π	
	1^-	0	10.48		11.60	0.38π	0.31π	
		1	10.76		15.41	0.54π	0.23π	
	2^+	0	10.55		12.81	0.43π	0.28π	
		1	10.61		15.80	0.58π	0.21π	
		2	10.68		14.70	0.52π	0.24π	
$^3\text{He}\,^4\text{HeAg}$	0^+	0	10.44	10.94	14.09	0.48π	0.27π	0.25π
		1	10.58	11.22	16.05	0.59π	0.22π	0.20π
	1^-	0	10.44	11.15	14.08	0.47π	0.28π	0.25π
	2^+	0	10.62	11.25	15.92	0.56π	0.23π	0.21π
		1	10.10	11.06	13.50	0.45π	0.29π	0.26π
$^3\text{He}_2\text{Ag}$	0^+	0		10.94	14.95	0.50π		0.25π
		1		11.24	16.18	0.57π		0.21π
	1^-	0		11.04	13.02	0.41π		0.30π
		1		11.76	15.16	0.47π		0.27π
	2^+	0		11.15	15.52	0.52π		0.24π
		1		11.37	15.62	0.52π		0.24π

probability density function defined by

$$\mathcal{D}(R, \theta, \varphi) = \int_0^{2\pi} d\alpha \int_0^{\pi} d\beta \int_0^{2\pi} d\gamma \,\sin 2\theta\, |\psi(R, \Omega)|^2. \tag{19}$$

We calculate the interparticle distances r_{12}, r_{23}, and r_{31} using Eq. (15) for each R, θ, and φ and sort the probability $\mathcal{D}(R, \theta, \varphi)$ into the pair distribution function $P(r)$, normalized as $\int_0^\infty P(r)dr = 1$. The angle distribution function $P(\vartheta)$ can be obtained similarly, by sorting the probability as a function
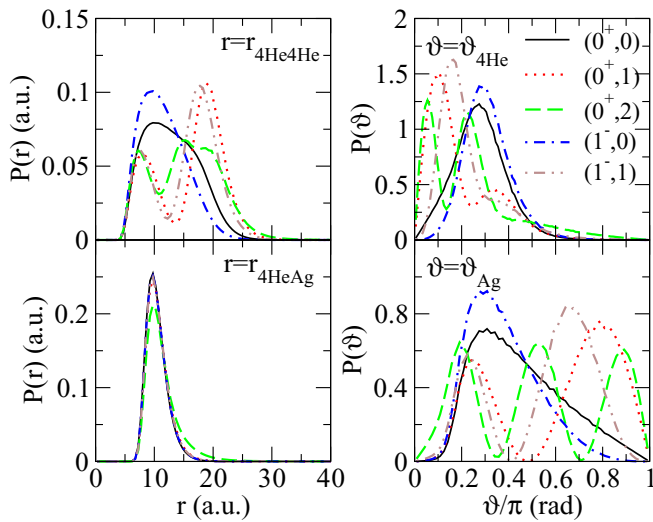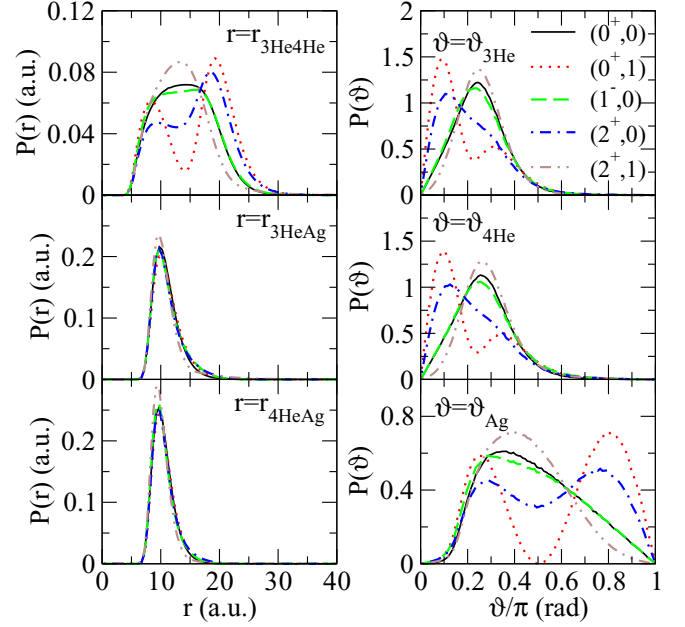

FIG. 3. Pair distributions $P(r)$ in the left column and angle distributions $P(\vartheta)$ in the right column for the $^4\text{He}_2\text{Ag}$ ground and excited-rovibrational states. The bound states are labeled as (J^Π, v), with J, Π, and v being, respectively, the total angular momentum, the parity, and the vibrational quantum number.

FIG. 4. Pair distributions $P(r)$ in the left column and angle distributions $P(\vartheta)$ in the right column for the $^3\text{He}\,^4\text{HeAg}$ ground and excited-rovibrational states.

of the bond angle $\vartheta_j = \cos^{-1}[(r_{ij}^2 + r_{jk}^2 - r_{kl}^2)/(2r_{ij}r_{jk})]$, and normalizing as $\int_0^\pi P(\vartheta)d\vartheta = 1$. The 1D distribution functions for the ground and several excited-rovibrational states of $^4\text{He}_2\text{Ag}$, $^3\text{He}\,^4\text{HeAg}$, and $^3\text{He}_2\text{Ag}$ are shown, respectively, in Figs. 3, 4, and 5, where the bound states are labeled (J^Π, v). All the pair and angle distribution functions display similar characteristics: the He-He pair distribution functions show one or two broad peaks up to $r \lesssim 25$ a.u., then decay and vanish at $r \approx 35$ a.u., while the He-Ag pair distribution functions peaks narrowly only once at around 10 a.u., decay, and vanish at $r \approx 20$ a.u. The He bond angle distributions present
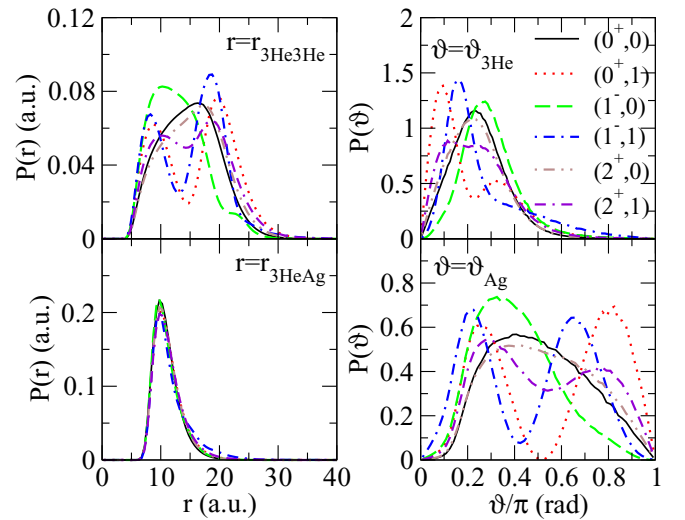

FIG. 5. Pair distributions $P(r)$ in the left column and angle distributions $P(\vartheta)$ in the right column for the $^3\text{He}_2\text{Ag}$ ground and excited-rovibrational states.
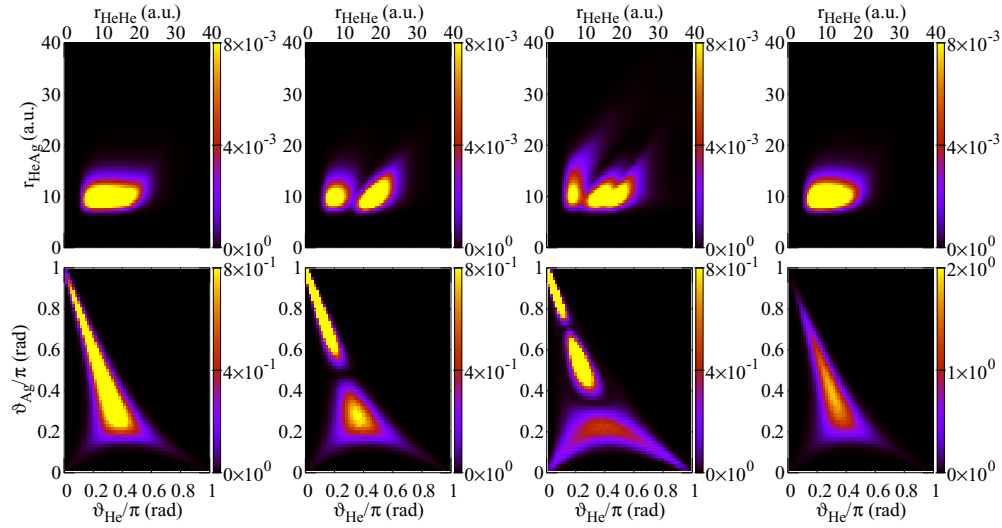
FIG. 6. Pair-pair distributions $P(r_{\mathrm{HeHe}}, r_{\mathrm{HeAg}})$ in the top row and angle-angle distributions $P(\vartheta_{\mathrm{He}}, \vartheta_{\mathrm{Ag}})$ in the bottom row for $^4\mathrm{He_2Ag}$. From the left to the right $(J^\Pi, v) = (0^+, 0)$, $(0^+, 1)$, $(0^+, 2)$, and $(1^-, 0)$ states are presented.

one or several narrow peaks up to $\vartheta \lesssim 0.4\pi$ and vanish at $\vartheta \approx 0.7\pi$-0.8π radians, whereas the Ag bond distribution functions extend all the way from $\vartheta = 0$ to π, displaying one or several broad maxima. From these pair and angle distribution functions, we can expect that the He-He-Ag complexes display various geometrical configurations with the He-Ag distances kept nearly fixed at some small distances and the Ag bond angle variable, which are close to obtuse isosceles triangles. These features can also be seen from the 2D pair-pair and angle-angel distribution functions, $P(r_{\mathrm{HeHe}}, r_{\mathrm{HeAg}})$ and $P(\vartheta_{\mathrm{He}}, \vartheta_{\mathrm{Ag}})$, calculated by sorting two distances and two angles from the 3D function (19), which are presented in Fig. 6 for selected bound states of $^4\mathrm{He_2Ag}$. The silver atom may locate preferably, not exactly but close to the line joining the two helium atoms. However, these He-He-Ag geometrical configurations are thought to be less variable than those shown by the helium trimers $\mathrm{He_3}$ [53], or the helium-helium-alkali-metal molecules [20], which are characterized by their very floppy nature. This difference stems from the fact that alkali atoms are much more loosely bound to the helium than are silver atoms. The present study might also explain the difference in the impurity locations between alkali-metals (located at the surface of) and silver atoms (located inside the helium nanodroplets), as was discussed in Sec. I.

IV. SUMMARY

In this work, we studied theoretically weakly bound triatomic $\mathrm{He_2Ag}$ molecules. Three different isotopic systems

$^4\mathrm{He_2Ag}$, $^3\mathrm{He}\,^4\mathrm{HeAg}$, and $^3\mathrm{He_2Ag}$, were considered with different total angular momenta J and parities Π. We calculated the energetics as well as the structural properties such as the 1D and 2D distribution functions. All the bound states are found to display similar structures: the helium and silver atoms are a little tightly bound at some nearly fixed distances, whereas the two helium atoms are more loosely bound at some variable distances to each other, with the He bond angles being more acute than the Ag bond angle. The silver atom may locate preferably, not exactly but very close to the line joining the two helium atoms, rather than outside them. Although still qualified as weakly bound species, these bound states can be considered simpler than the extremely floppy $\mathrm{He_3}$ or $\mathrm{He_2Li}$ bound states due to the rather tight nature of the He-Ag interaction. The triatomic complexes containing helium and other coinage metals, gold and copper, are other interesting subjects of study. Our further goal is to simulate, within our three-body hyperspherical formalism, the three-body collision processes $\mathrm{Ag} + \mathrm{He} + \mathrm{He} \leftrightarrow \mathrm{AgHe} + \mathrm{He}$, relevant to the buffer-gas experiments mentioned above in this work.

[1] V. Efimov, Phys. Lett. B **33**, 563 (1970).

[2] V. Efimov, Nucl. Phys. A **210**, 157 (1973).

[3] P. Naidon and S. Endo, Rep. Prog. Phys. **80**, 056001 (2017).

[4] C. H. Greene, P. Giannakeas, and J. Pérez-Ríos, Rev. Mod. Phys. **89**, 035006 (2017).

[5] E. A. Kolganova, A. K. Motovilov, and W. Sandhas, Few-Body Syst. **51**, 249 (2011).

[6] E. A. Kolganova, A. K. Motovilov, and W. Sandhas, Few-Body Syst. **58**, 35 (2017).

[7] M. Kunitski, S. Zeller, J. Voigtsberger, A. Kalinin, L. P. H. Schmidt, M. Schöffler, A. Czasch, W. Schöllkopf,

R. E. Grisenti, T. Jahnke, D. Blume, and R. Dörner, Science **348**, 551 (2015).

[8] T. Lim, S. K. Duffy, and W. C. Damer, Phys. Rev. Lett. **38**, 341 (1977).

[9] B. D. Esry, C. D. Lin, and C. H. Greene, Phys. Rev. A **54**, 394 (1996).

[10] D. Blume, C. H. Greene, and B. D. Esry, J. Chem. Phys. **113**, 2145 (2000).

[11] H. Suno and B. D. Esry, Phys. Rev. A **78**, 062701 (2008).

[12] J. Yuan and C. D. Lin, J. Phys. B: At. Mol. Opt. Phys. **31**, L637 (1998).

[13] A. Delfino, T. Frederico, and L. Tomio, J. Chem. Phys. **113**, 7874 (2000).

[14] I. Baccarelli, G. Delgado-Barrio, F. A. Gianturco, T. Gonzalez-Lezana, S. Miret-Artés, and P. Villarreal, Europhys. Lett. **50**, 567 (2000).

[15] I. Baccarelli, G. Delgado-Barrio, F. A. Gianturco, T. González-Lezana, S. Miret-Artes, and P. Villarreal, Phys. Chem. Chem. Phys. **2**, 4067 (2000).

[16] C. D. Paola, F. A. Gianturco, F. Paesani, G. Delgado-Barrio, S. Miret-Artés, P. Villarreal, I. Baccarelli, and T. González-Lezana, J. Phys. B: At. Mol. Opt. Phys. **35**, 2643 (2002).

[17] H. Suno and B. D. Esry, Phys. Rev. A **82**, 062521 (2010).

[18] P. Stipanović, L. V. Markić, I. Bešlić, and J. Boronat, Phys. Rev. Lett. **113**, 253401 (2014).

[19] M.-S. Wu, H.-L. Han, C.-B. Li, and T.-Y. Shi, Phys. Rev. A **90**, 062506 (2014).

[20] H. Suno, Phys. Rev. A **96**, 012508 (2017).

[21] P. Stipanović, L. Vranješ Markić, D. Zarić, and J. Boronat, J. Chem. Phys. **146**, 014305 (2017).

[22] E. Kolganova and V. Roudnev, Few-Body Syst. **60**, 32 (2019).

[23] Q. Gou and Y. Li, Phys. Rev. A **85**, 012510 (2012).

[24] D. López-Durán, R. Rodríguez-Cantano, T. González-Lezana, G. Delgado-Barrio, P. Villarreal, and F. A. Gianturco, Phys. Rev. A **86**, 022501 (2012).

[25] D. López-Durán, R. Rodríguez-Cantano, T. González-Lezana, G. Delgado-Barrio, P. Villarreal, and F. A. Gianturco, Eur. Phys. J. D **66**, 198 (2012).

[26] J. P. Toennies and A. F. Vilesov, Angew. Chem., Int. Ed. **43**, 2622 (2004).

[27] S. Grebenev, J. P. Toennies, and A. F. Vilesov, Science **279**, 2083 (1998).

[28] F. Stienkemeier and A. F. Vilesov, J. Chem. Phys. **115**, 10119 (2001).

[29] M. Choi, G. Douberly, T. Falconer, W. Lewis, C. Lindsay, J. Merritt, P. Stiles, and R. Miller, Int. Rev. Phys. Chem. **25**, 15 (2006).

[30] R. N. Barnett and K. B. Whaley, Phys. Rev. A **47**, 4082 (1993).

[31] F. Ancilotto, E. Cheng, M. W. Cole, and F. Toigo, Z. Phys. B **98**, 323 (1995).

[32] F. Ancilotto, P. B. Lerner, and M. W. Cole, J. Low Temp. Phys. **101**, 1123 (1995).

[33] F. Stienkemeier, F. Meier, and H. Lutz, J. Chem. Phys. **107**, 10816 (1997).

[34] A. Hernando, R. Mayol, M. Pi, M. Barranco, F. Ancilotto, O. Bünermann, and F. Stienkemeier, J. Phys. Chem. A **111**, 7303 (2007).

[35] A. Bartelt, J. D. Close, F. Federmann, N. Quaas, and J. P. Toennies, Phys. Rev. Lett. **77**, 3525 (1996).

[36] F. Federmann, K. Hoffmann, N. Quaas, and J. D. Close, Phys. Rev. Lett. **83**, 2548 (1999).

[37] M. Mella, M. C. Colombo, and G. Morosi, J. Chem. Phys. **117**, 9695 (2002).

[38] A. Wada, T. Takayanagi, and M. Shiga, J. Chem. Phys. **119**, 5478 (2003).

[39] N. Brahms, T. V. Tscherbul, P. Zhang, J. Kłos, H. R. Sadeghpour, A. Dalgarno, J. M. Doyle, and T. G. Walker, Phys. Rev. Lett. **105**, 033001 (2010).

[40] T. N. Rescigno and C. W. McCurdy, Phys. Rev. A **62**, 032706 (2000).

[41] C. Lin, Phys. Rep. **257**, 1 (1995).

[42] O. I. Tolstikhin, S. Watanabe, and M. Matsuzawa, J. Phys. B: At. Mol. Opt. Phys. **29**, L389 (1996).

[43] H. Suno, J. Chem. Phys. **134**, 064318 (2011).

[44] H. Suno, J. Chem. Phys. **135**, 134312 (2011).

[45] H. Suno, B. D. Esry, C. H. Greene, and J. P. Burke, Phys. Rev. A **65**, 042725 (2002).

[46] R. C. Whitten and F. T. Smith, J. Math. Phys. **9**, 1103 (1968).

[47] M. Abramowitz and I. A. Stegun, *Handbook of Mathematical Functions with Formulas, Graphs, and Mathematical Tables*, 9th Dover Printing, 10h GPO Printing ed. (Dover, New York, 1964).

[48] C. de Boor, *A Practical Guide to Splines* (Springer, New York, 1978).

[49] R. A. Aziz and M. J. Slaman, J. Chem. Phys. **94**, 8047 (1991).

[50] J. C. Xie, S. K. Mishra, T. Kar, and R.-H. Xie, Chem. Phys. Lett. **605-606**, 137 (2014).

[51] A. M. Gardner, R. J. Plowright, M. J. Watkins, T. G. Wright, and W. H. Breckenridge, J. Chem. Phys. **132**, 184301 (2010).

[52] K. Baluja, P. Burke, and L. Morgan, Comput. Phys. Commun. **27**, 299 (1982).

[53] H. Suno, J. Phys. B: At. Mol. Opt. Phys. **49**, 014003 (2016).